Results in Physics 6 (2016) 627–633

Contents lists available at ScienceDirect

Results in Physics

journal homepage: www.journals.elsevier.com/results-in-physics

Boundary layer flow of Maxwell fluid in rotating frame with binary chemical reaction and activation energy

Z. Shafique [a], M. Mustafa [a,*], A. Mushtaq [b]

[a] School of Natural Sciences (SNS), National University of Sciences and Technology (NUST), Islamabad 44000, Pakistan
[b] Research Centre for Modeling and Simulation (RCMS), National University of Sciences and Technology (NUST), Islamabad 44000, Pakistan

ARTICLE INFO

Article history:
Received 30 August 2016
Accepted 8 September 2016
Available online 16 September 2016

Keywords:
Maxwell fluid
Activation energy
Chemical reaction
Numerical solution
Rotating frame
Stretching sheet

ABSTRACT

Here we study the heat/mass transfer effects on revolving flow of Maxwell fluid due to unidirectional stretching surface. Mass transfer process is modeled in terms of binary chemical reaction and activation energy. Modified Arrhenius function for activation energy is invoked. Traditional boundary layer approximations are utilized to simplify the governing equations. Using similarity method, self-similar form of boundary layer equations are derived which are solved numerically. The solutions depend on dimensionless numbers such as the rotation parameter λ, the Deborah number β, the Prandtl number Pr, the Schmidt number Sc, activation energy E, fitted rate constant n and temperature difference parameter δ. We found that the solute concentration in binary mixture is proportional to both rotation parameter λ and activation energy E. The reaction rate σ and fitted rate n both provide reduction in the solute concentration. Thermal boundary layer becomes thicker and heat transfer rate diminishes when fluid is subjected to a larger rotation rate.

Introduction

Mass transfer is a natural phenomenon in many processes such as absorption, vaporization and condensation in a mixture, diffusion of nutrients in tissues, thermal insulation, cooling towers and food processing, in absorbers such as activated carbon beds and in the condensation process, dispersion of temperature/moisture over groove fields and distillation of alcohol. Mass transfer has relevance in most living-matter processes such as respiration, nutrition, sweating etc. Mass transfer process with chemical reaction has been given special attention in the past (see [1–6] and ref. there in) because of its significance in chemical engineering, geothermal reservoirs, nuclear reactor cooling and thermal oil recovery. Bestman [7] was probably the first to study the boundary layer flow involving the binary chemical reaction. He analytically examined the effects of the activation energy on natural convection flow in a porous medium by using perturbation approach. One of the factors that have an important role in chemical reaction is the activation energy. It is defined as the least obligatory amount of energy for atoms or molecules to bring themselves in a state in which they can undergo a chemical reaction. The concept of activation energy is usually applicable in areas pertaining to geothermal or oil reservoir engineering and mechanics of water and oil emulsions. Activation energy can be realized as energy barrier that separates two minima of potential energy (of the reactants and products of a reaction) which has to be overcome by reactants to initiate a chemical reaction. Makinde et al. [8] presented the numerical solution for unsteady convection flow over a flat porous plate with nth order chemical reaction and Arrhenius activation energy. The recent attempts in this direction were made by Maleque [9,10] who investigated the influence of binary chemical reaction with Arrhenius activation energy on mixed convection flows and Awad et al. [11] who explored the unsteady revolving flow due to impulsively stretched plate by means of spectral relaxation method (SRM).

Steady and unsteady rotating flows have several noteworthy applications in geophysical and chemical fluid dynamics. They are also of applied significance in many areas such as in food processing, in rotor–stator systems, in thermal-power generating systems, in rotating machinery and in the cooling of the skins of high speed aircrafts. Wang [12] firstly explored the mathematical model for the effects of rotation on fluid flow adjacent to a stretched plate. In his work analytical solutions of velocity and temperature profiles were derived by perturbation approach. Effects of magnetic field on rotating fluid flow on stretching plate were observed by Takhar et al. [13]. Nazar et al. [14] employed similarity approach to examine unsteady revolving flow by an impulsively stretching

* Corresponding author.
E-mail address: meraj_mm@hotmail.com (M. Mustafa).

http://dx.doi.org/10.1016/j.rinp.2016.09.006
2211-3797/

plate. Kumari et al. [15] considered the flow near a stretching plate in revolving power-law and derived numerical approximations for both pseudoplastic and dilatant type fluids. Local similarity solutions for rotating viscous flow due to exponentially stretching plate were obtained by Javed et al. [16] utilizing Keller-box method. Zaimi et al. [17] considered a stretching surface immersed in rotating Walters' B liquid. Mustafa [18] analytically studied the rotating flow of viscoelastic fluid bounded by a stretching surface through Cattaneo-Christov heat flux theory. Turkyilmazoglu [19] performed a numerical study for MHD flow due to rotating shrinking disk. In another attempt, Turkyilmazoglu [20] extended the traditional Bödewadt flow problem for uniformly stretching disk. His numerical solution through collection method showed that radial stretching of disk improves the cooling process in practical applications. Mustafa et al. [21] also studied the Bödewadt flow problem over a stretching disk utilizing nanofluids. Numerical simulations for rotating flow of water containing ferromagnetic particles were reported by Mustafa et al. [22]. Rosali et al. [23] discussed the rotational effects on flow past an exponentially shrinking sheet and observed multiplicity of solutions in case of injection. Ahmad and Mustafa [24] performed a comparative study for revolving flow of nanofluids using two different thermal conductivity models and convective conditions. Imtiaz et al. [25] explored the flow of carbon nanotubes between radially stretching disks by a homotopic approach. An exact solution for flow simultaneously caused by coaxially rotating stretchable disks was presented by Turkyilmazoglu [26].

In this paper, we aim to explore the influences of binary chemical reaction with activation energy on rotating flow of Maxwell fluid over a stretchable surface. Coriolis and centrifugal effects attributed due to the fluid rotation are preserved in the mathematical model. Using similarity approach, self-similar solutions for velocity, temperature and concentration are developed. Graphical illustrations for velocity, temperature and concentration are presented to emphasize the physical effects of embedded parameters on the solutions. Numerical values of local Nusselt number and local Sherwood number for a broad range of parameters are tabulated.

Mathematical model

Consider a three-dimensional flow of an incompressible Maxwell fluid over an elastic surface located in the xy-plane. The fluid resides in the space $z \geqslant 0$. The surface is stretched in the x-direction with the linearly varying velocity of the form $u_w(x) = ax$ which induces flow in the neighboring layers of the fluid. Let Ω be the constant angular velocity of the rotating fluid. The surface is kept at constant temperature T_w and solute concentration at the surface is denoted by C_w. Let T_∞ and C_∞ be the ambient values of temperature and solute concentration respectively. Physical sketch of the problem is shown in Fig. 1. Governing equations in the presence of species chemical reaction with Arrhenius activation energy are expressed below (see Awad et al. [11] for details):

$$\nabla \cdot \mathbf{V} = 0, \tag{1}$$

$$\rho\,[(\mathbf{V}\cdot\nabla)\mathbf{V} + (\boldsymbol{\Omega}\times(\boldsymbol{\Omega}\times\mathbf{r})) + (2\boldsymbol{\Omega}\times\mathbf{V})] = -\nabla p + \nabla\cdot\mathbf{S}, \tag{2}$$

$$\rho c_p(\mathbf{V}\cdot\nabla T) = k\nabla^2 T, \tag{3}$$

$$(\mathbf{V}\cdot\nabla C) = D\nabla^2 C - k_r^2\left(\frac{T}{T_\infty}\right)^n e^{-\frac{E_a}{kT}}(C - C_\infty), \tag{4}$$

where k is the thermal conductivity, D the solute diffusivity, ρ the fluid density, c_p the specific heat and $\boldsymbol{\Omega} = [0, 0, \Omega]$ the angular velocity vector. The term $\boldsymbol{\Omega}\times(\boldsymbol{\Omega}\times\mathbf{r}) = -\nabla\left(\Omega^2 r^2/2\right)$ represents the centrifugal force which is being balanced by the pressure gradient

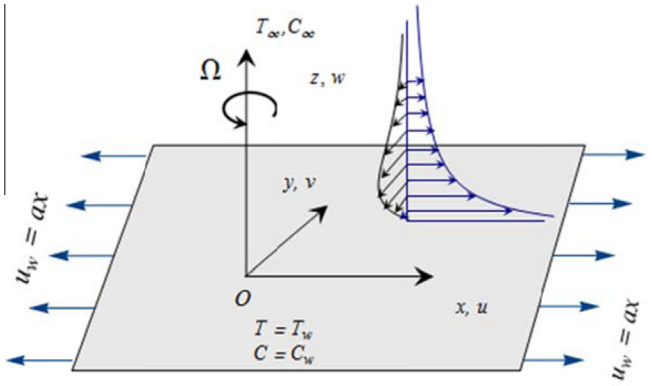

Fig. 1. Physical configuration and coordinate system.

$-\nabla p$. The term $k_r^2(T/T_\infty)^n e^{-\frac{E_a}{kT}}$ is the modified Arrhenius function [11] in which $\kappa = 8.61\times10^{-5}$ eV/K is the Boltzmann constant, k_r^2 the reaction rate and n the fitted rate constant generally lies in $-1 < n < 1$. In Eq. (2), $\mathbf{S}$ is the extra stress tensor for upper-convected Maxwell fluid which satisfies the following:

$$\mathbf{S} + \lambda_1\frac{D\mathbf{S}}{Dt} = \mu\mathbf{A}_1,$$

in which λ_1 is the fluid relaxation time, $\mathbf{A_1} = (\nabla\mathbf{V}) + (\nabla\mathbf{V})^t$ the first Rivlin–Ericksen tensor and D/Dt the upper-convected time derivative. Invoking the conventional boundary layer approximations, Eqs. (1)–(4) can be expressed in component forms as below:

$$\frac{\partial u}{\partial x} + \frac{\partial v}{\partial y} + \frac{\partial w}{\partial z} = 0, \tag{5}$$

$$\begin{aligned} u\frac{\partial u}{\partial x} + v\frac{\partial u}{\partial y} + w\frac{\partial u}{\partial z} - 2\Omega v &= \nu\left(\frac{\partial^2 u}{\partial z^2}\right) \\ &- \lambda_1\begin{bmatrix} u^2\frac{\partial^2 u}{\partial x^2} + v^2\frac{\partial^2 u}{\partial y^2} + w^2\frac{\partial^2 u}{\partial z^2} \\ +2uv\frac{\partial^2 u}{\partial x\partial y} + 2vw\frac{\partial^2 u}{\partial y\partial z} + 2uw\frac{\partial^2 u}{\partial x\partial z} \\ -2\Omega\left(u\frac{\partial v}{\partial x} + v\frac{\partial v}{\partial y} + w\frac{\partial v}{\partial z}\right) + 2\Omega\left(v\frac{\partial u}{\partial x} - u\frac{\partial u}{\partial y}\right) \end{bmatrix}, \end{aligned} \tag{6}$$

$$\begin{aligned} u\frac{\partial v}{\partial x} + v\frac{\partial v}{\partial y} + w\frac{\partial v}{\partial z} + 2\Omega u &= \nu\left(\frac{\partial^2 v}{\partial z^2}\right) \\ &- \lambda_1\begin{bmatrix} u^2\frac{\partial^2 v}{\partial x^2} + v^2\frac{\partial^2 v}{\partial y^2} + w^2\frac{\partial^2 v}{\partial z^2} \\ +2uv\frac{\partial^2 v}{\partial x\partial y} + 2vw\frac{\partial^2 v}{\partial y\partial z} + 2uw\frac{\partial^2 v}{\partial x\partial z} \\ +2\Omega\left(u\frac{\partial u}{\partial x} + v\frac{\partial u}{\partial y} + w\frac{\partial u}{\partial z}\right) + 2\Omega\left(v\frac{\partial v}{\partial x} - u\frac{\partial v}{\partial y}\right) \end{bmatrix}, \end{aligned} \tag{7}$$

$$u\frac{\partial T}{\partial x} + v\frac{\partial T}{\partial y} + w\frac{\partial T}{\partial z} = \alpha\frac{\partial^2 T}{\partial z^2}, \tag{8}$$

$$u\frac{\partial C}{\partial x} + v\frac{\partial C}{\partial y} + w\frac{\partial C}{\partial z} = D\nabla^2 C - k_r^2\left(\frac{T}{T_\infty}\right)^n e^{-\frac{E_a}{kT}}(C - C_\infty). \tag{9}$$

The boundary conditions in the present problem are:

$$\begin{aligned} &u = ax,\ v = 0,\ w = 0,\ T = T_w,\ C = C_w \quad \text{at } z = 0, \\ &u \to 0,\ v \to 0,\ T \to T_\infty,\ C \to C_\infty \quad \text{as } z \to \infty. \end{aligned} \tag{10}$$

We introduce the following set of similarity variables involving dimensionless vertical distance η as

$$\begin{aligned} &\eta = \sqrt{\frac{a}{\nu}}z,\ u = axf'(\eta),\ v = axg(\eta),\ w = -\sqrt{a\nu}f(\eta), \\ &\theta = \frac{T - T_\infty}{T_w - T_\infty},\ \phi = \frac{C - C_\infty}{C_w - C_\infty}, \end{aligned} \tag{11}$$

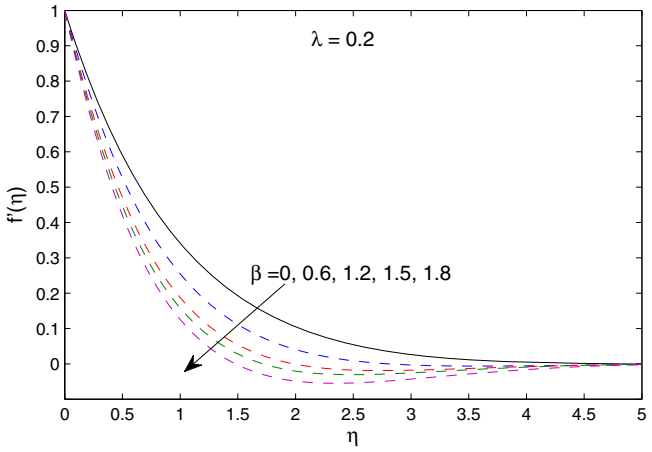

Fig. 2. Effect of β on $f'(\eta)$.

Eq. (5) is automatically satisfied and Eqs. (6)–(9) convert into the following ordinary differential equations:

$$f''' + ff'' - f'^2 + 2\lambda(g - \beta fg') + \beta[2ff'f'' - f^2 f'''] = 0, \tag{12}$$

$$g'' + fg' - f'g - 2\lambda\left[f' + \beta\left(f'^2 - ff'' + g^2\right)\right] + \beta\left[2ff'g' - f^2 g''\right] = 0, \tag{13}$$

$$\frac{1}{Pr}\theta'' + f\theta' = 0, \tag{14}$$

$$\frac{1}{Sc}\phi'' + f\phi' - \sigma[1+\delta\theta]^n \exp\left[-\frac{E}{1+\delta\theta}\right]\phi = 0, \tag{15}$$

subject to the transformed conditions

$$\begin{aligned} &\text{at } \eta = 0: \ f = g = 0, \ f' = 1, \ \theta = \phi = 1, \\ &\text{as } \eta \to \infty: \ f' \to 0, \ g \to 0, \ \theta \to 0, \ \phi \to 0. \end{aligned} \tag{16}$$

where $\lambda = \Omega/a$ is the rotation parameter, $\beta = \lambda_1 a$ the Deborah number, $Pr = \mu c_p/k$ the Prandlt number, $Sc = \nu/D$ the Schmidt number, $E = E_a/(\kappa T_\infty)$ the non-dimensional activation energy, $\delta = (T_w - T_\infty)/T_\infty$ the temperature difference parameter, $\sigma = k_r^2/a$ the dimensionless reaction rate.

Fourier law can be used to define local Nusselt number Nu_x and Fick's law can be employed to define local Sherwood number Sh_x. These are as follows:

$$Nu_x = \frac{xq_w}{k(T_w - T_\infty)}, \ Sh_x = \frac{xj_w}{D(C_w - C_\infty)}, \tag{17}$$

where q_w is the wall heat flux and j_w is the wall mass flux given by

$$q_w = -k\left.\frac{\partial T}{\partial z}\right|_{z=0}, \ j_w = -D\left.\frac{\partial C}{\partial z}\right|_{z=0}. \tag{18}$$

Now using Eq. (11) and Eq. (18), Eq. (17) becomes

$$\frac{Nu_x}{\sqrt{Re_x}} = -\theta'(0), \ \frac{Sh_x}{\sqrt{Re_x}} = -\phi'(0), \tag{19}$$

where $Re_x = ax^2/\nu$ is the local Reynolds number.

Numerical method

Here we deal with the numerical solutions of Eqs. (12)–(15) with the conditions (16) by conventional shooting approach. We convert Eqs. (12)–(16) into a system of first order equations by writing $f = x_1, f' = x_2, f'' = x_3, g = x_4, g' = x_5, \theta = x_6, \theta' = x_7, \phi = x_8, \phi' = x_9$. We obtain the following:

$$\begin{bmatrix} x_1' \\ x_2' \\ x_3' \\ x_4' \\ x_5' \\ x_6' \\ x_7' \\ x_8' \\ x_9' \end{bmatrix} = \begin{bmatrix} x_2 \\ x_3 \\ \left(x_2^2 - x_1x_3 - 2\lambda(x_4 - \beta x_1x_5) - 2\beta x_1x_2x_3\right)/(1 - \beta x_1^2/2) \\ x_5 \\ \left(x_2x_4 - x_1x_5 + 2\lambda(x_2 + \beta(x_2^2 - x_1x_3 + x_4^2)) - 2\beta x_1x_2x_5)\right)(1 - \beta x_1^2/2) \\ x_7 \\ -Prx_1x_7 \\ x_9 \\ Sc(\sigma[1+\delta x_6]^n \exp[-E/(1+\delta x_6)]x_8 - x_1x_9) \end{bmatrix}, \tag{20}$$

with the following initial conditions

$$\begin{bmatrix} x_1(0) \\ x_2(0) \\ x_3(0) \\ x_4(0) \\ x_5(0) \\ x_6(0) \\ x_7(0) \\ x_8(0) \\ x_9(0) \end{bmatrix} = \begin{bmatrix} 0 \\ 1 \\ u_1 \\ 0 \\ u_2 \\ 1 \\ u_3 \\ 1 \\ u_4 \end{bmatrix}, \tag{21}$$

where $[u_1, u_2, u_3, u_4] = [f''(0), g'(0), \theta'(0), \phi'(0)]$. The first order system (20) can be integrated numerically through fifth-order Runge–Kutta method by assigning appropriate values to u_1, u_2, u_3 and u_4. Newton–Raphson method is implemented to iteratively estimate these values. The whole process is repeated at different $\eta_{\max}$ say $\eta = 10, 11, 12, 13$ until the solutions exponentially tend to free stream conditions with specified tolerance say 10^{-5}. The obtained solutions are found to be consistent with those from the MATLAB built in routine *bvp4c*.

Results and discussion

In this section, our focus is to analyze the role of embedded parameters on the velocity, temperature and concentration profiles. First of all, we compare our findings of $f''(0)$ with those of previously published papers in absence of fluid rotation (see Table 1). The results are found in very good agreement for all considered

Table 1
Comparison with $-f''(0)$ obtained by Abel et al. [27], Megahed [28] and Abbasi et al. [29] for different values of β in absence of fluid rotation, that is, $\lambda = 0$.

β	Abel et al. [27]	Megahed [28]	Abbasi et al. [29]	Present results
0.0	0.999962	0.999978	1.00000	1.000000
0.2	1.051948	1.051945	1.05189	1.051887
0.4	1.101850	1.101848	1.10190	1.101898
0.6	1.150163	1.150160	1.15014	1.150128
0.8	1.196692	1.196690	1.19671	1.196708
1.2	1.285257	1.285253	1.28536	1.285361
1.6	1.368641	1.368641	1.36873	1.368756
2.0	1.447617	1.447616	1.44781	1.447648

values of Deborah number β. Fig. 2 preserves the influence of Deborah number β on the velocity field f' when $\lambda = 0.2$. The profiles indicate a decreasing trend in f' for increasing values of β. It means that fluid motion in the x-direction is opposed by the viscoelastic effects. For larger values of β, the profiles of f' tend to zero at smaller distances above the sheet. In smaller Deborah number fluid, viscous effect is dominant compared to the elastic effect whereas the fluid tends to behave as elastically solid material when Deborah number enlarges. In Fig. 3, the influence of rotation parameter λ on the velocity in x-direction is observed. The rotational effects tend to slow down the fluid motion in the x-direction. For smaller λ, the decrease in velocity field f' with η is monotonic while an interesting oscillatory behavior in f' is observed for large λ which

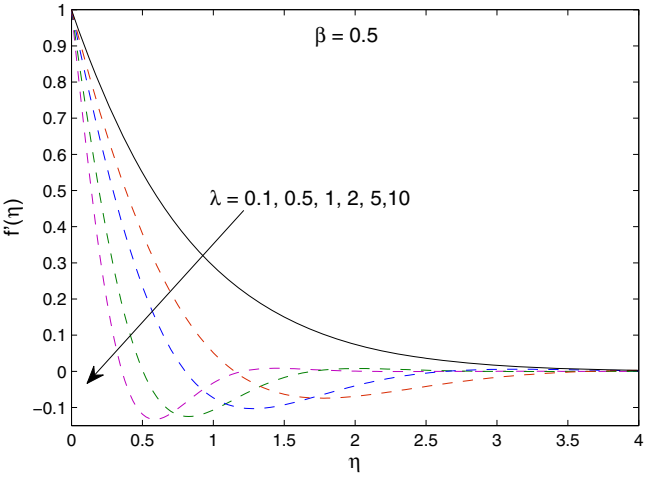

Fig. 3. Effect of λ on $f'(\eta)$.

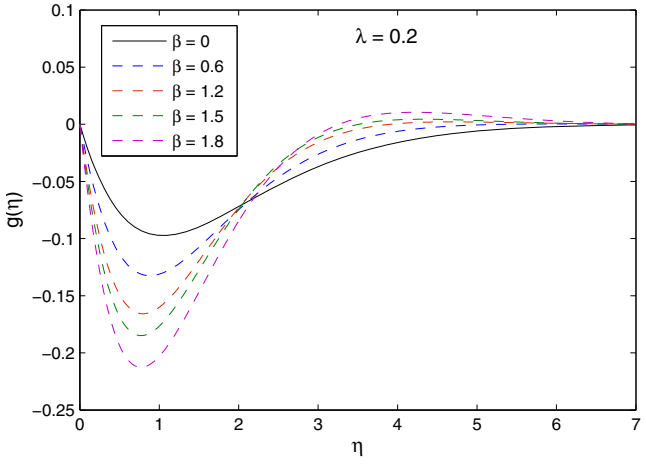

Fig. 4. Effect of β on $g(\eta)$.

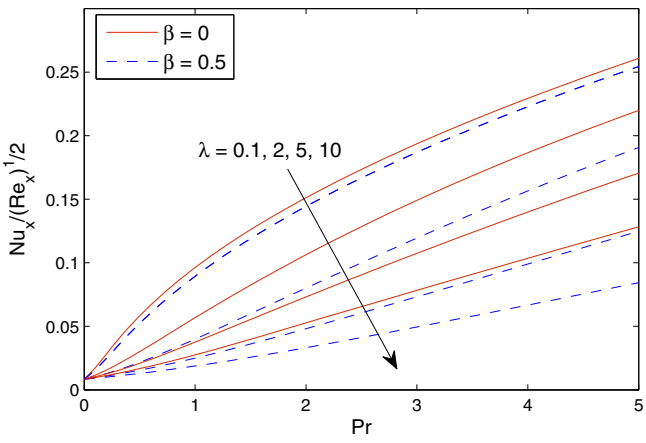

Fig. 5. Effect of Pr and λ on $Nu_x/\sqrt{\mathrm{Re}_x}$ for $\beta = 0$ and $\beta = 0.5$.

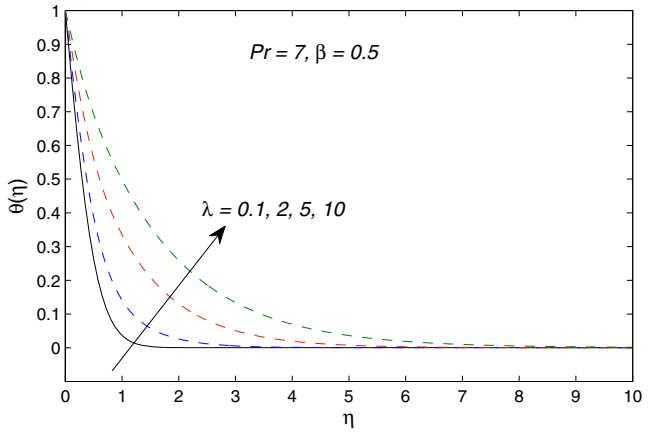

Fig. 6. Effect of λ on $\theta(\eta)$.

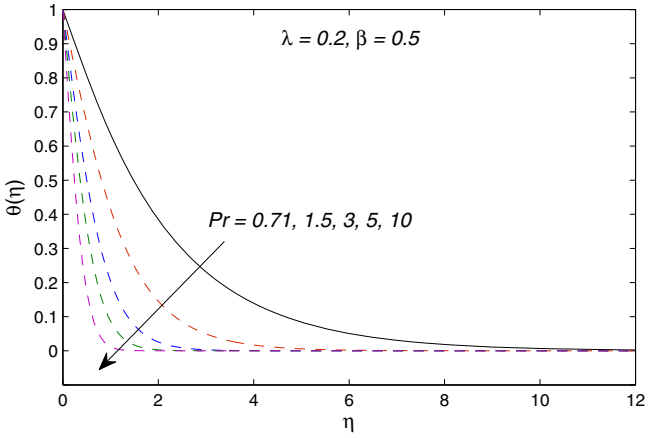

Fig. 7. Effect of Pr on $\theta(\eta)$.

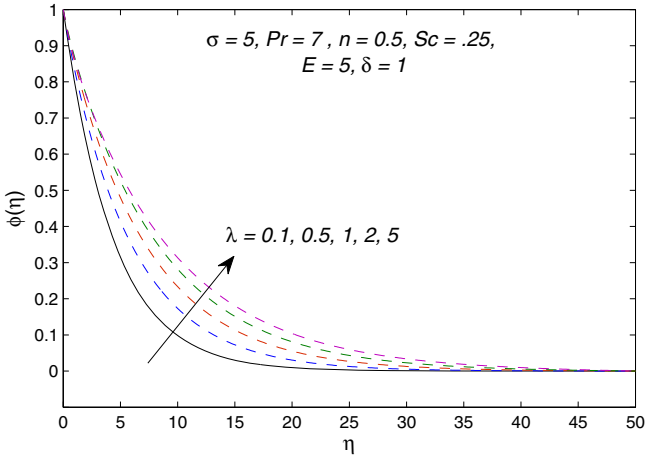

Fig. 8. Effect of λ on $\phi(\eta)$.

is due to the rotational effects. Fig. 4 shows the profiles of g for various values of Deborah number β with $\lambda = 0.2$. The negative value of g reveals that flow is solely in the negative y-direction. For a larger value of λ, the oscillations in the profile of g analogous to those of f' are observed.

Fig. 5 is presented to analyze the influence of rotation on the local Nusselt number which determines the heat transfer rate from the sheet. It is observed that the local Nusselt number approaches zero for vanishing Prandtl number Pr and it increases upon increasing Pr. It is also clear that local Nusselt number has inverse relationship with λ. It means that the heat transfer rate reduces when fluid is subjected to a larger rotation rate. In Fig. 6 we have plotted temperature field θ for different values of parameter λ. Temperature θ increases and thermal boundary layer becomes thicker upon increasing the parameter λ. Physically it is attributed to the fact that the larger rotation parameter λ gives larger kinetic energy to the fluid which enhances its temperature. Fig. 7 shows the relation between Prandtl number Pr and temperature θ. Larger Prandtl number implies weaker thermal diffusivity that leads to thinner penetration depth of temperature.

In Fig. 8, the effects of rotation parameter λ on the concentration profile $\phi(\eta)$ have been shown. It depicts that concentration boundary layer thickness grows when angular velocity Ω is increased. Concentration profiles for various values of dimensionless activation energy E have been plotted in Fig. 9. It reveals that increasing the dimensionless activation energy causes the thickening of the concentration boundary layer. This is because low temperature and high activation energy leads to smaller reaction rate constant and thus slow down the chemical reaction. Consequently, the concentration of the solute increases. Fig. 10 shows the variation in solute concentration with the variation in temperature difference parameter δ. It is observed that solute concentration ϕ is a decreasing function of δ. This implies that concentration boundary layer

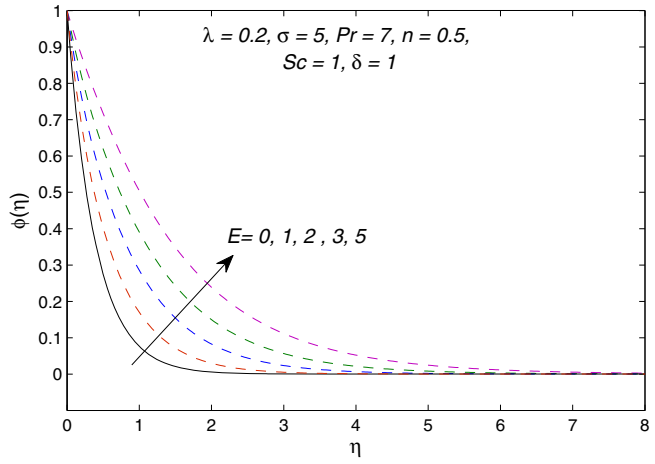

Fig. 9. Effect of E on $\phi(\eta)$.

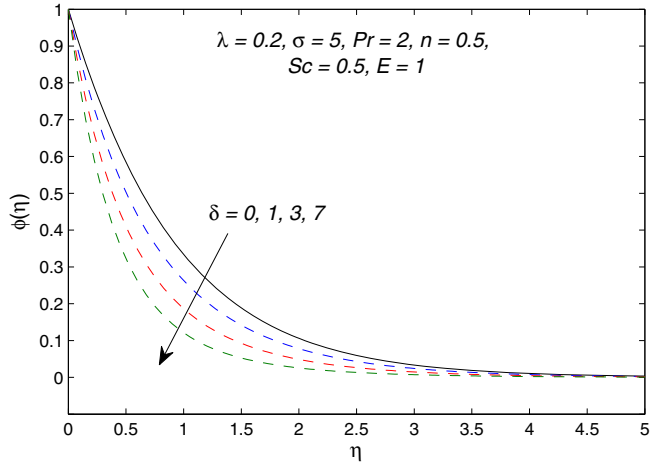

Fig. 10. Effect of δ on $\phi(\eta)$.

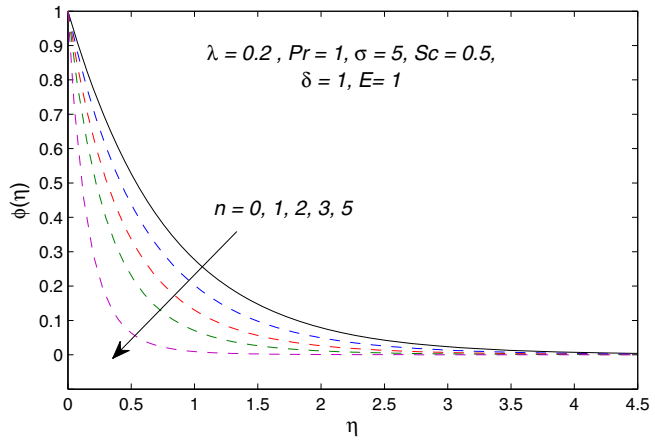

Fig. 11. Effect of n on $\phi(\eta)$.

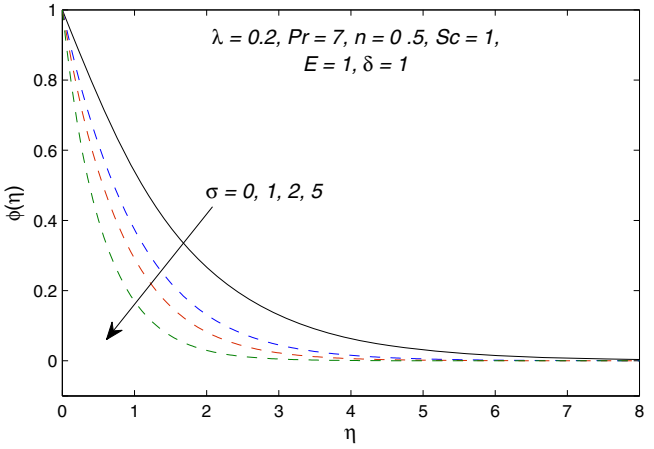

Fig. 12. Effect of σ on $\phi(\eta)$.

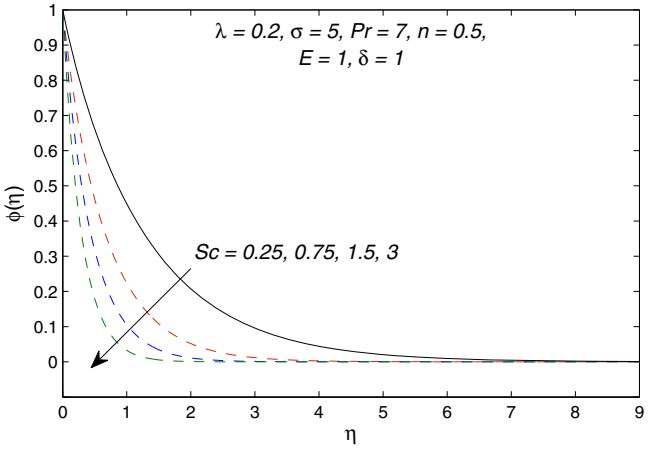

Fig. 13. Effect of Sc on $\phi(\eta)$.

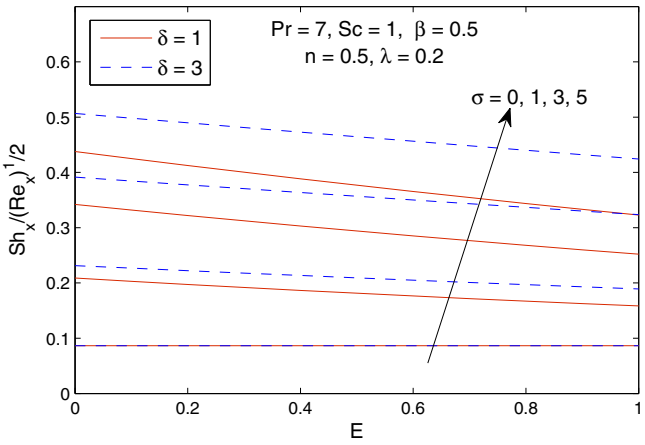

Fig. 14. Effect of E and σ on $Sh_x/\sqrt{\mathrm{Re}_x}$ for $\delta = 1$ and $\delta = 3$.

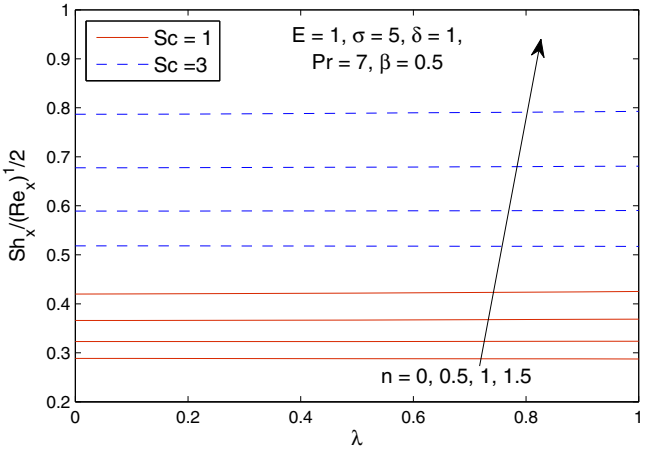

Fig. 15. Effect of λ and n on $Sh_x/\sqrt{\mathrm{Re}_x}$ for $Sc = 1$ and $Sc = 3$.

thickness increases when difference between wall and ambient temperature enlarges. Figs. 11 and 12 are prepared to observe the influence of fitted rate constant n and reaction rate σ on solute concentration ϕ respectively. It can be observed that an increase in either n or σ results in an increase in the factor $\sigma(1+\delta\theta)^n \exp(-E/1+\delta\theta)$. This eventually favors the destructive chemical reaction due to which concentration rises. The reduction in ϕ is accompanied with a larger concentration gradient at the wall. The effects of Schimdt number Sc on concentration profile can be noticed from Fig. 13. It illustrates the thinning of concentration boundary layer when Sc is increased. Physically, an increase in Schmidt number Sc corresponds to lower solute diffusivity which results in shorter penetration depth of concentration.

Plots of local Sherwood number $\mathrm{Re}_x^{-1/2}Sh_x$ versus activation energy at different values of reaction rate constant have been included in Fig. 14. There is a decrease in as E increases and this decrease is pronounced when larger values of σ are employed. It means that mass flux from the sheet is smaller when chemical reaction requires larger activation energy. Fluid rotation rate seems to have a mild influence on the wall mass flux for any prescribed values of n and Sc (see Fig. 15). The magnitude of $\mathrm{Re}_x^{-1/2}Sh_x$ is increased when Schmidt number Sc is varied from $Sc = 1$ to $Sc = 3$.

Tables 2 and 3 are presented to observe the trends in wall heat and mass transfer rates with the variation in embedded

Table 2
Numerical values of local Nusselt number $-\theta'(0)$ for various values of λ, Pr and β.

λ	β	Pr	$-\theta'(0)$
0.2	0.5	1	0.51903
1.0			0.34237
1.5			0.27827
2.0			0.23746
0.2	0.2	1	0.54670
	0.4		0.52809
	0.6		0.51009
	0.8		0.49255
0.2	0.5	2	0.85109
		5	1.51553
		7	1.84540
		10	2.26033

Table 3
Numerical values of local Sherwood number $-\phi'(0)$ for different values of Sc, λ, E and σ.

Sc	λ	E	σ	$-\phi'(0)$
1	0.2	1	1	0.95064
3				1.80760
5				2.40990
8				3.12064
1	0.1	1	1	0.95576
	1			0.90663
	2			0.88791
	3			0.88577
1	0.2	2	1	0.75333
		4		0.58015
		6		0.53528
		8		0.52368
0.2	0.2	1	1.5	0.43149
			2.0	0.49336
			2.5	0.54928
			3	0.60083

parameters. Table 2 shows that magnitude of local Nusselt number $\mathrm{Re}_x^{-1/2}Nu_x$ decreases as the rotation parameter λ and Deborah number β increase while it significantly grows as Prandtl number Pr increases. In other words, fluid rotation and viscoelasticity have adverse impact on the cooling process of the sheet. Table 3 indicates a sharp growth in local Sherwood number $\mathrm{Re}_x^{-1/2}Sh_x$ when either Schmidt number Sc or reaction rate constant σ is incremented. Schmidt number compares the momentum diffusion to mass diffusion. Thus concentration boundary layer becomes thinner and mass transfer rate augments when Sc increases.

Concluding remarks

A mathematical model is analyzed to investigate the consequences of Arrhenius activation energy and binary chemical reaction on the flow of Maxwell fluid in a rotating frame. Numerical solutions are developed by shooting method. The key observations of this work are outlined below:

1. Velocities in the x- and y-directions decrease as fluid relaxation time λ_1 increases. Also, wall heat flux reduces upon increasing the fluid relaxation time λ_1.
2. Hydrodynamic boundary layer thins when rotation parameter λ is incremented. An oscillatory behavior in both x- and y-components of velocity is observed when rotation parameter λ is sufficiently large.
3. The vertical component of velocity at far field decreases when either Deborah number β or rotation parameter λ is increased.
4. Thermal boundary layer significantly grows when fluid rotates at larger angular velocity. This growth is accompanied with a reduction in wall slope of temperature and eventually the local Nusselt number.

5. Solute concentration ϕ increases and wall mass flux reduces when a larger rotation parameter λ is employed.
6. Activation energy E enhances the solute concentration and reduces wall mass flux. This reduction grows further when difference between wall and ambient temperatures is increased.
7. Solute concentration ϕ is found to reduce when reaction rate constant σ enlarges. Concentration ϕ is also inversely proportional to the temperature differences.
8. Schmidt number Sc decreases the solute concentration and supports the mass transfer rate from the wall.

References

[1] Chamkha AJ, Rashad AM, Al-Mudhaf H. Heat and mass transfer from truncated cones with variable wall temperature and concentration in the presence of chemical reaction effects. Int J Numer Meth Heat Fluid Flow 2012;22:357–76.
[2] Mallikarjuna B, Rashad AM, Chamkha AJ, Raju SH. Chemical reaction effects on MHD convective heat and mass transfer flow past a rotating vertical cone embedded in a variable porosity regime. Afrika Matematika 2015;27:645–65.
[3] Zhang C, Zheng L, Zhang X, Chen G. MHD flow and radiation heat transfer of nanofluids in porous media with variable surface heat flux and chemical reaction. Appl Math Model 2015;39:165–81.
[4] Khan N, Mahmood T, Sajid M, Hashmi MS. Heat and mass transfer on MHD mixed convection axisymmetric chemically reactive flow of Maxwell fluid driven by exothermal and isothermal stretching disks. Int J Heat Mass Transf 2016;92:1090–105.
[5] Mabood F, Shateyi S, Rashidi MM, Momoniat E, Freidoonimehr N. MHD stagnation point flow heat and mass transfer of nanofluids in porous medium with radiation, viscous dissipation and chemical reaction. Adv. Powder Technol. 2016;27:742–9.
[6] Rawat S, Kapoor S, Bhargava R. MHD flow heat and mass transfer of micropolar fluid over a nonlinear stretching sheet with variable micro inertia density, heat flux and chemical reaction in a non-darcy porous medium. J. Appl. Fluid Mech. 2016;9:321–31.
[7] Bestman. Natural convection boundary layer with suction and mass transfer in a porous medium. Int J Eng Res 1990;14:389–96. http://dx.doi.org/10.1002/er.4440140403.
[8] Makinde OD, Olanrewaju PO, Charles WM. Unsteady convection with chemical reaction and radiative heat transfer past a flat porous plate moving through a binary mixture. Africka Matematika 2011;22:65–78. http://dx.doi.org/10.1007/s13370-011-0008-z.
[9] Maleque KA. Effects of binary chemical reaction and activation energy on MHD boundary layer heat and mass transfer flow with viscous dissipation and heat generation/absorption. ISRN Thermodyn 2013. http://dx.doi.org/10.1155/2013/284637. Article ID 284637.
[10] Maleque KA. Effects of exothermic/endothermic chemical reactions with Arrhenius activation energy on MHD free convection and mass transfer flow in presence of thermal radiation. J Thermodyn 2013. http://dx.doi.org/10.1155/2013/692516. Article ID 692516.
[11] Awad FG, Motsa S, Khumalo M. Heat and mass transfer in unsteady rotating fluid flow with binary chemical reaction and activation energy. PLoS ONE 2014;9(9):e107622. http://dx.doi.org/10.1371/journal.pone.0107622.
[12] Wang CY. Stretching a surface in a rotating fluid. J Appl Math Phys (ZAMP) 1988;39:177–85.
[13] Takhar HS, Chamkha AJ, Nath G. Flow and heat transfer on a stretching surface in a rotating fluid with a magnetic field. Int J Therm Sci 2003;42:23–31.
[14] Nazar R, Amin N, Pop I. Unsteady boundary layer flow due to a stretching surface in a rotating fluid. Mech. Res. Commun. 2004;31:121–8.
[15] Kumari M, Grosan T, Pop I. Rotating flows of power-law fluids over a stretching surface. Technische Mechanik 2006;1:11–9.
[16] Zaimi K, Ishak A, Pop I. Stretching surface in rotating viscoelastic fluid. Appl Math Mech 2013;34:945–52.
[17] Javed T, Sajid M, Abbas Z, Ali N. Non-similar solution for rotating flow over an exponentially stretching surface. Int J Numer Meth Heat Fluid Flow 2011;21:903–8.
[18] Mustafa M. Cattaneo-Christov heat flux model for rotating flow and heat transfer of upper-convected Maxwell fluid. AIP Adv. 2015;5:047109. http://dx.doi.org/10.1063/1.4917306.
[19] Turkyilmazoglu M. MHD fluid flow and heat transfer due to a shrinking rotating disk. Comput Fluids 2014;90:51–6.
[20] Turkyilmazoglu M. Bödewadt flow and heat transfer over a stretching stationary disk. Int J Mech Sci 2015;90:246–50.
[21] Mustafa M, Khan JA, Hayat T, Alsaedi A. On Bödewadt flow and heat transfer of nanofluids over a stretching stationary disk. J Mol Liq 2015;211:119–25.
[22] Mustafa M, Mushtaq A, Hayat T, Alsaedi A. Rotating flow of magnetite-water nanofluid over a stretching surface inspired by non-linear thermal radiation. PLoS ONE 2016;11. http://dx.doi.org/10.1371/journal.pone.0149304.
[23] Rosali H, Ishak A, Nazar R, Pop I. Rotating flow over an exponentially shrinking sheet with suction. J Mol Liq 2015;211:965–9.
[24] Ahmad R, Mustafa M. Model and comparative study for rotating flow of nanofluids due to convectively heated exponentially stretching sheet. J Mol Liq 2016;220:635–41.
[25] Imtiaz M, Hayat T, Alsaedi A, Ahmad B. Convective flow of carbon nanotubes between rotating stretchable disk with thermal radiation effects. Int J Heat Mass Transf 2016;101:948–57.
[26] Turkyilmazoglu M. Flow and heat simultaneously induced by two stretchable rotating disks. AIP Phys Fluids 2016;28. http://dx.doi.org/10.1063/1.4945651. Article ID 043601.
[27] Abel MS, Tawade JV, Nandeppanavar MM. MHD flow and heat transfer for the upper-convected Maxwell fluid over a stretching sheet. Meccanica 2012;47:385–93.
[28] Megahed AM. Variable fluid properties and variable heat flux effects on the flow and heat transfer in a non-Newtonian Maxwell fluid over an unsteady stretching sheet with slip velocity. Chin Phys B 2013;22. http://dx.doi.org/10.1088/1674-1056/22/9/094701. Article ID 094701.
[29] Abbasi FM, Mustafa M, Shehzad SA, Alhuthali MS, Hayat T. Analytical study of Cattaneo-Christov heat flux model for a boundary layer flow of Oldroyd-B fluid. Chin Phys B 2016;25. http://dx.doi.org/10.1088/1674-1056/25/1/014701. Article ID 014701.